Crustal architecture and deep structure of the Ninetyeast Ridge hotspot trail from active-source ocean bottom seismology

I. Grevemeyer,[1,2] E. R. Flueh,[2] C. Reichert,[3] J. Bialas,[2] D. Kläschen[2] and C. Kopp[2]

[1] *FB Geowissenschaften, Universität Bremen, Klagenfurterstrasse, 28359 Bremen, Germany. E-mail: ingo@geophys2.uni-bremen.de*

[2] *GEOMAR, Forschungszentrum für Marine Geowissenschaften, Wischhofstrasse 1–3, 24148 Kiel, Germany*

[3] *Bundesanstalt für Geowissenschaften und Rohstoffe, Postfach 51 01 53, 30631 Hannover, Germany*

SUMMARY

A 550-km-long transect across the Ninetyeast Ridge, a major Indian ocean hotspot trail, provided seismic refraction and wide-angle reflection data recorded on 60 ocean bottom instruments. About 24 000 crustal and 15 000 upper mantle arrivals have been picked and used to derive an image of the hotspot track. Two approaches have been chosen: (i) a first-arrival tomographic inversion yielding crustal properties; and (ii) forward modelling of mantle phases revealing the structure at the crust–mantle boundary region and of the uppermost mantle. Away from the volcanic edifice, seismic recordings show the typical phases from oceanic crust, that is, two crustal refraction branches (*Pg*), a wide-angle reflection from the crust–mantle boundary (*PmP*) and a wave group turning within the upper mantle (*Pn*). Approaching the edifice, three additional phases have been detected. We interpret these arrivals as a wide-angle reflection from the base of material trapped under the pre-hotspot crust (*Pm₂P*) and as a wide-angle reflection (*PnP*) and its associated refraction branch (*P_N*) from a layered upper mantle.

The resulting models indicate normal oceanic crust to the west and east of the edifice. Crustal thickness averages 6.5–7 km. Wide-angle reflections from both the pre-hotspot and the post-hotspot crust–mantle boundary suggest that the crust under the ridge has been bent downwards by loading the lithosphere, and hotspot volcanism has underplated the pre-existing crust with material characterized by seismic velocities intermediate between those of mafic lower crustal and ultramafic upper mantle rocks (7.5–7.6 km s^{-1}). In total, the crust is up to ≈ 24 km thick. The ratio between the volume of subcrustal plutonism forming the underplate and extrusive and intrusive volcanism forming the edifice is about 0.7. An important observation is that underplating continued to the east under the Wharton Basin. During the shield-building phase, however, Ninetyeast Ridge was located adjacent to the Broken Ridge and was subsequently pulled apart along a transform fault boundary. Therefore, underplating eastwards of the fracture zone separating the edifice from the Wharton Basin suggests that prolonged crustal growth by subcrustal plutonism occurred over millions of years after the major shield-building stage. This fact, however, requires mantle flow along the fossil hotspot trail. The occurrence of *PnP* and *P_N* arrivals is probably associated with a layered and anisotropic upper mantle due to the preferential alignment of olivine crystals and may have formed by rising plume material which spread away under the base of the lithosphere.

Key words: hotspots, large igneous provinces, melt generation, refraction seismology, seismic velocities.

1 INTRODUCTION

Large igneous provinces (LIPs) are voluminous emplacements of predominantly mafic extrusive and intrusive rocks whose origins lie in processes usually not related to plate tectonics; they are often interpreted as a consequence of enhanced melting due to a mantle plume (e.g. Coffin & Eldholm 1992, 1994). LIPs are believed to be the physical manifestation of global mantle processes and include continental flood basalts, volcanic passive margins, oceanic plateaus and submarine ridges or seamount chains. While continental flood basalts, volcanic passive margins and oceanic plateaus are generally associated with massive

outbursts of igneous activity occurring episodically in Earth's history (e.g. Larson 1991; Coffin & Eldholm 1994), submarine ridges and seamount chains indicate mantle fluxes distributed more or less evenly in time. Many submarine ridges follow emplacement of continental flood basalts or oceanic plateaus in time; for example, the Chagos–Laccadive Ridge which shares the source, now beneath La Réunion, which created the Deccan Traps and the Mascarene Plateau (Duncan & Richards 1991; White & McKenzie 1989), or the Ninetyeast Ridge, which together with the Kerguelen Plateau and Broken Ridge and the Rajmahal Traps had a common source, now located beneath the Kerguelen and Heard Islands (Mahoney *et al.* 1983; Kent *et al.* 1997). Thus, it seems reasonable to suggest that giant oceanic plateaus and continental flood basalt provinces are the result of the initiation or impact of a new plume head reaching the base of the lithosphere (e.g. Campbell & Griffiths 1990), while submarine ridges and seamount chains present the manifestation of an established mantle plume in terms of the Wilson (1963) and Morgan (1971) models.

The study of LIPs, however, is directly related to the understanding of mantle dynamics and associated magmatic processes. Models of melt generation allow the prediction of melt composition and suggest that the seismic structure of the crust and upper mantle is a good indicator of the magmatic processes related to the emplacement of LIPs (White & McKenzie 1989; Keleman & Holbrook 1995).

The Ninetyeast Ridge is a major Indian Ocean hotspot track and was created in Late Cretaceous and Early Tertiary times by the Kerguelen hotspot. The ridge can be traced for about 5000 km from latitude 30°S, where it joins Broken Ridge, northwards into the Bay of Bengal, where it is buried beneath the Bengal Fan (Fig. 1). Palaeontological, palaeomagnetic, and radiometric analysis of rock samples from Deep Sea Drilling Project (DSDP) legs 22 and 26 and Ocean Drilling Program (ODP) leg 121 indicated that basement ages become older in the northward direction from approximately 38 Ma at DSDP site 254 near the southern terminus of the ridge to between 80 and 82 Ma at the most northerly ODP site 758 (Peirce 1978; Duncan 1991; Royer *et al.* 1991). The obliquity of Ninetyeast Ridge relative to the fracture zone pattern of the Indian Basin and the occurrence of an Eocene extinct spreading centre in the Wharton Basin to the east suggest that the northern part of Ninetyeast Ridge was emplaced by intraplate volcanism, whereas the middle and southern parts were emplaced along a transform plate boundary (Royer *et al.* 1991) separating Ninetyeast Ridge and Broken Ridge. This setting provided the unique opportunity to study the timing between extrusive volcanism and clastic processes forming the volcanic edifice and clastic apron and intrusive magmatism at the base of the crust forming a subcrustal plutonic core complex or underplating body. Thus, if extrusive and/or underplated material occur eastward of Ninetyeast Ridge and hence to the east of the transform plate boundary, late stage magmatism occurred millions of years after Ninetyeast Ridge was created and subsequently pulled apart from Broken Ridge.

In the Spring of 1998, multibeam bathymetry and seismic reflection, refraction and wide-angle data were collected aboard the German research vessel SONNE (Flueh & Reichert 1998;
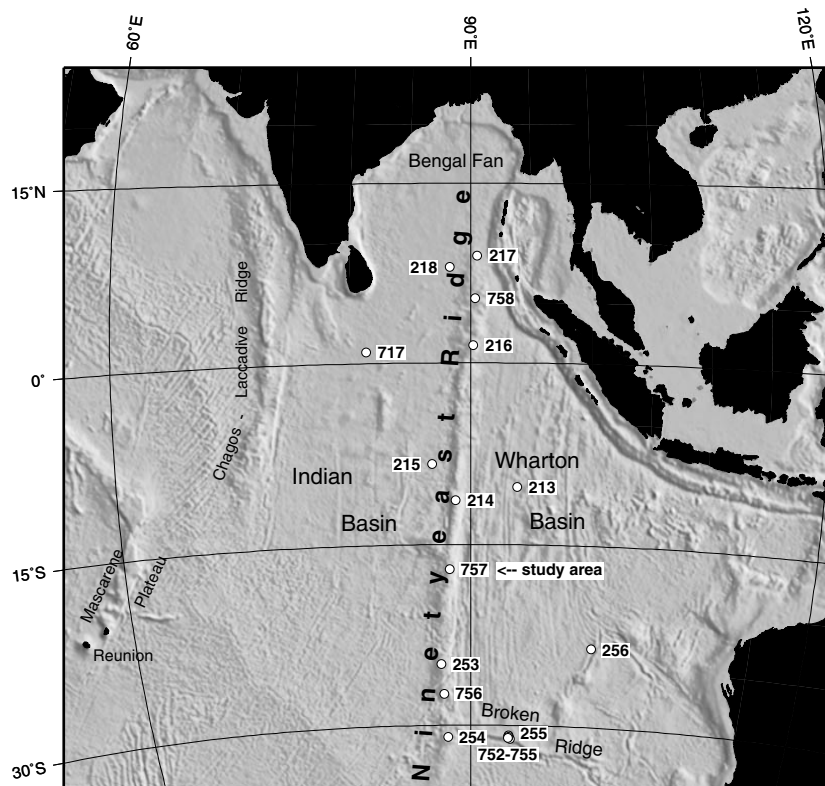

Figure 1. Illuminated predicted seafloor topography (Smith & Sandwell 1997) showing the main structural features of the central Indian ocean and the Ninetyeast Ridge, created between ≈90 and 38 Ma above the Kerguelen mantle plume (Royer *et al.* 1991). Also shown are Deep Sea Drilling Project (DSDP) and Ocean Drilling Program (ODP) sites drilled on and adjacent to Ninetyeast Ridge. The study area was located in the vicinity of ODP site 757 (Peirce *et al.* 1989). Figs 1, 7 and 11(a) may be viewed in colour in the online version of the journal (www.blackwell-synergy.com).

Flueh *et al.* 1999a) on Ninetyeast Ridge near 17°S. The study area was centred on ODP site 757 drilled during ODP leg 121 (Peirce *et al.* 1989). A detailed description of the morphology and shallow structure of Ninetyeast Ridge is presented elsewhere (Flueh & Reichert 1998; Flueh *et al.* 1998, 1999b; Grevemeyer *et al.* 1999). In this paper, we use a 550-km-long seismic refraction and wide-angle reflection transect across the ridge to yield the crustal architecture and the deep crustal and upper mantle structure of the hotspot trail. The results reveal insight into the melt generation, mantle flow and stages of magmatic construction over a hotspot plume. Implications of crustal underplating on the state of isostasy and the subsidence history of Ninetyeast Ridge are discussed by Grevemeyer & Flueh (2000).

2   SEISMIC EXPERIMENT

During R/V *Sonne* cruise 131, a large ocean bottom seismograph (OBS) and hydrophone (OBH) experiment was conducted on Ninetyeast Ridge (Flueh & Reichert 1998; Flueh *et al.* 1999a). In total about 2500 km of seismic refraction/ wide-angle and seismic reflection data have been acquired including the deployment and successful recovery of more than 100 OBHs and OBSs and the use of a three-channel ministreamer (Fig. 2). The kernel was a network of profiles in an area approximately 55 km by 110 km around ODP site 757 and a roughly 550-km-long east–west transect through its centre. The aim was to study the small-scale structure of the volcanic edifice (Flueh *et al.* 1999b) and the regional structure of the hotspot trail and adjacent ocean basins.

In this paper we present results from the transect which extends from the Indian Basin across Ninetyeast Ridge into the Wharton Basin. The transect is composed of three profiles, each about 300 km long (Figs 3–6). To simulate a single refraction line the profiles were shot with an overlap of 100–150 km. On profile numbers 05, 06 and 31, we deployed 25, 25 and 15 ocean bottom stations, respectively (Fig. 6). The instruments were digital recording hydrophones and seismographs of GEOMAR (Flueh & Bialas 1996; Bialas & Flueh 1999). In total, 60 instruments provided data for geophysical data analyses and inversion.

The seismic source was a tuned array of 20 airguns providing a total volume of 51.2 l. The shot interval was 60 s, resulting in an average shot spacing of 110 m. Data passed an anti-aliasing filter of 50 Hz and were continuously recorded with a sampling rate of 200 Hz on all OBH and OBS stations. The data were played back and split into single-shot records stored as a receiver

gather in SEG-Y format. The instruments were deployed by free fall, using Global Positioning System (GPS) for drop-point positioning; instrument locations were further constrained using water-path traveltimes from the shots collected while the ship was navigated with GPS. Spectral analysis and filter tests show that the seismic energy is in a band ranging from 5 to 30 Hz. We ran this test for both near-offset and far-offset traces and chose a time- and range-dependent filtering approach. In addition, amplitudes were multiplied by distance to compensate partly for the spherical divergence, simultaneously showing the level of both seismic signal and ambient noise.

3   SEISMIC DATA

Figs 3 to 5 show typical examples of the OBH data. The most relevant features of the recordings are two clear crustal branches *Pg*, which are evident on all stations. Shots westwards of instruments in the Indian Basin and instruments in the Wharton Basin indicate all the phases typical of oceanic crust, that is, a wide-angle reflection from the crust–mantle boundary *PmP* and an upper mantle refraction branch, *Pn*. Stations on the Ninetyeast Ridge provided up to four additional phases, which can emerge even at large offsets of ≈ 110 km. In terms of previous studies on other hotspot edifices, we interpreted those phases as reflections from the base of pre-hotspot oceanic crust (*PmP*) and the base of an underplating body or post-hotspot Moho (Watts *et al.* 1985; ten Brink & Brocher 1987; Caress *et al.* 1995; Charvis *et al.* 1999). We call this underplating phase Pm_2P. Additionally, the data provided strong evidence for a reflector, *PnP*, and refractor, P_N, deeper in the lithosphere. Similar arrivals have been observed under other major hotspot islands (Gallart *et al.* 1999; Smallwood *et al.* 1999; Ye *et al.* 1999) and elsewhere in oceanic crust (LADLE Study Group 1983; Pavlenkova 1996).

3.1   Crustal arrivals

All instruments allow a detailed resolution of the edifice and of crustal rock adjacent to the ridge. Stations in the Indian and Wharton basins show upper crustal phases at up to 5–12 km shot–receiver offset (Fig. 3a). First arrivals can be correlated with apparent velocities in the range 3.5–5.5 km s^{-1}, typical of basaltic rocks (White *et al.* 1992; Grevemeyer & Weigel 1996). Approaching the ridge, upper crustal phases show up out to a 20 km shot–receiver offset (Fig. 4a), indicating a thickening of the volcanic lava pile.
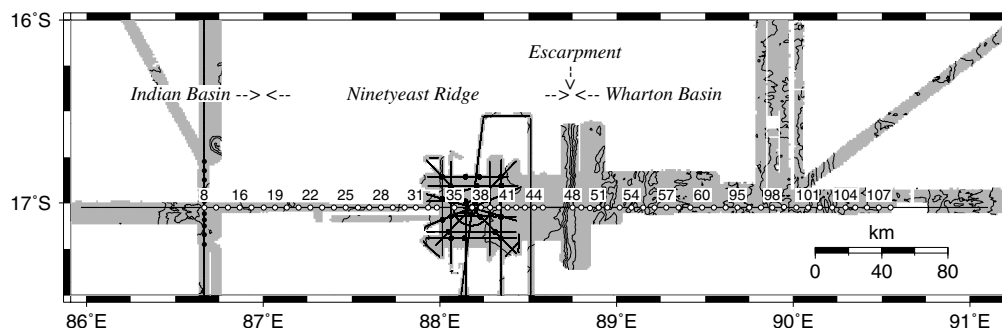

Figure 2. Map showing seismic survey lines obtained during RV *Sonne* cruise 131 (Flueh & Reichert 1998). Along the 550-km-long transect across Ninetyeast Ridge, 60 ocean bottom receivers (white dots) provided data used in traveltime inversion and modelling.
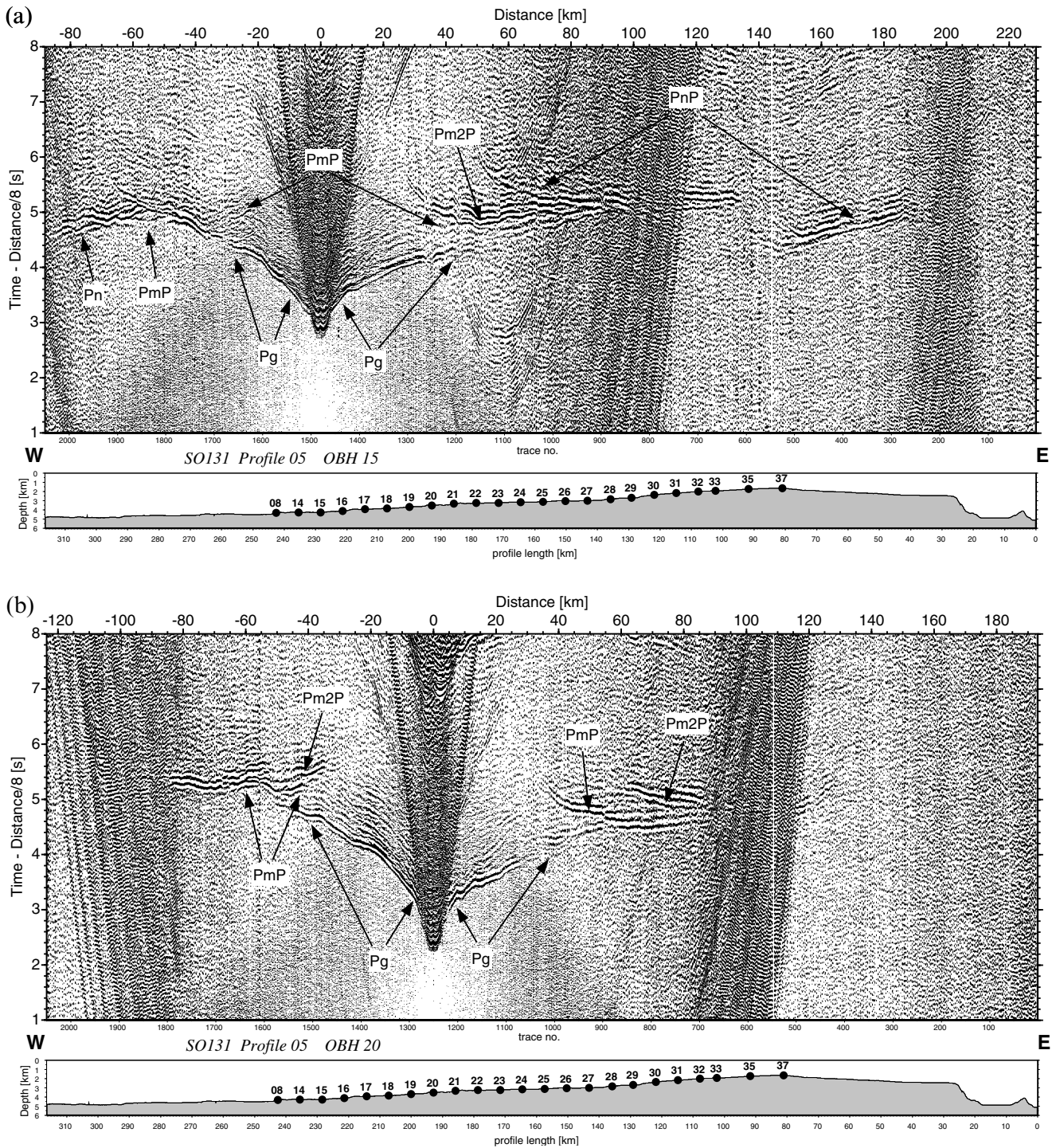
Figure 3. Hydrophone data from airgun shots over (a) OBH 15 (b) OBH 20 (c) OBH 26 and (d) OBH 28 on profile 05. Seismograms have been processed with a time- and offset-dependent filtering approach and scaled by range. *Pg*: crustal arrivals; *PmP*: wide-angle reflection from the base of pre-hotspot crust; *Pm₂P*: wide-angle reflection from the base of the underplating body; *Pn*: energy turning within the uppermost mantle; *PnP*: wide-angle reflection from a layered upper mantle and *P_N*: associated refraction branch. Sections are plotted with a reduction velocity of 8 km s^{-1}.

The second crustal refraction branch has apparent velocities of 6.5–7.2 km s^{-1} and corresponds to gabbroic rock, typical of oceanic layer 3 (White *et al.* 1992). Like the upper crustal refraction branch, typical lower crustal velocities can be observed out to larger shot–receiver distances on the edifice than within the basins (90–100 km versus 40–50 km, respectively), suggesting that the thicknesses of both the upper and lower crust increase

towards the edifice. In Figs 3 to 5 we have labelled both crustal phases as *Pg*.

Traveltime uncertainties of picked arrivals vary between 10 and 80 ms. Within the Wharton Basin, however, diffraction and scattering from a rough seabed often make it difficult to identify the exact onset time of *P*-waves, thus uncertainties here can reach values of ≈ 100 ms.
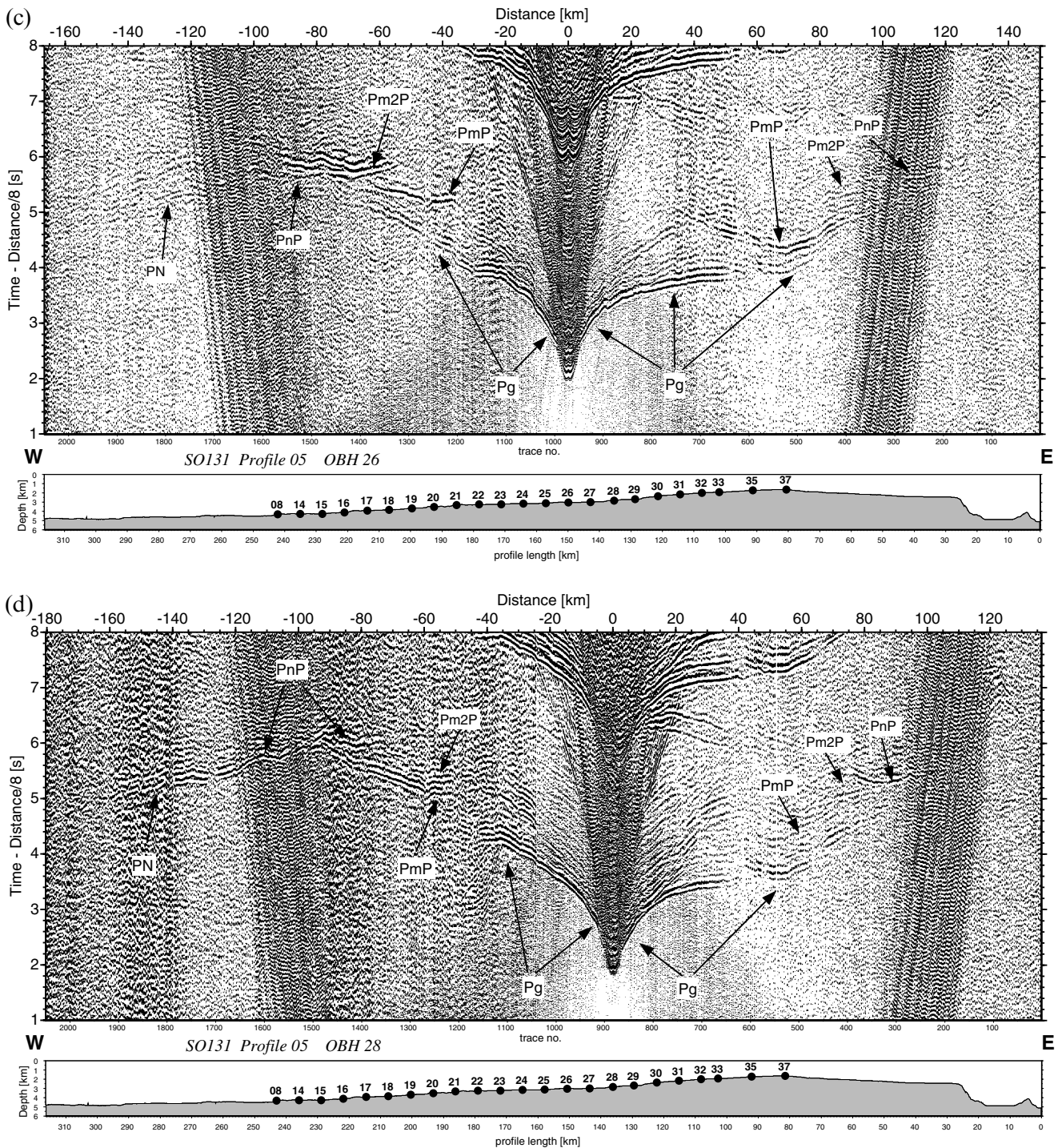
(c)

(d)

Figure 3. (*Continued.*)

3.2 Arrivals from the crust–mantle boundary region

Wide-angle reflections from the crust–mantle boundary or *PmP* arrivals are evident on oceanic crust adjacent to the ridge. They can be observed on the westernmost instruments from profile 05 and in the Wharton Basin along profile 31 (Figs 3a, 4c and 5). Additionally, these instruments provided *Pn* arrivals. Approaching the ridge, we use the term *PmP* for the first wide-angle reflection phase occurring, and therefore representing the base of pre-hotspot oceanic crust. A second phase, called Pm_2P may represent the base of material added by hotspot volcanism at the base of the crust, i.e. underplated material (Figs 3a–d). Both phases could be observed on several instruments, although features and amplitudes change from instrument to instrument and may indicate layering and heterogeneities in the crust–mantle boundary region. Traveltimes could be picked with uncertainties of 50–120 ms.
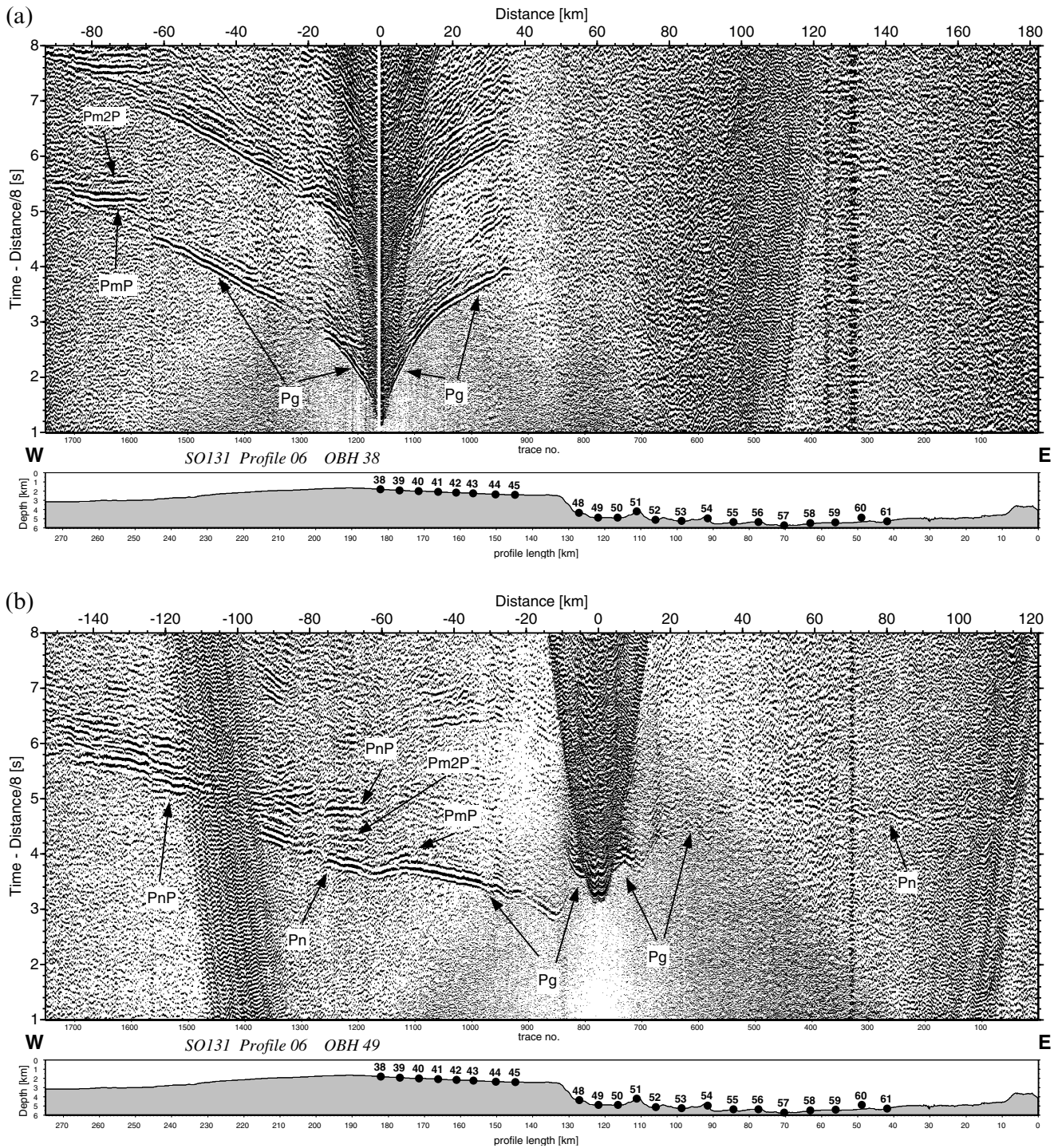
(a)

SO131 Profile 06 OBH 38

(b)

SO131 Profile 06 OBH 49

Figure 4. Hydrophone data from airgun shots over (a) OBH 38 (b) OBH 49 and (c) OBH 58 on profile 06. Data processing and phases as in Fig. 3.

3.3 Deep mantle arrivals

A strong wide-angle reflection arrival (PnP) and associated refraction branch (P_N) occur in several record sections (Figs 3a and d and 4a and b). These arrivals are associated with energy turning not in the crust–mantle boundary region, but deeper in the lithosphere. Apparent velocities clearly exceed 8.0 km s^{-1}, although the topography is dipping away from the OBHs. Thus, the arrivals are related to a high-velocity layer at sub-Moho level. Traveltime uncertainties vary between 70 and 120 ms.

4 METHODOLOGY

We chose two approaches to yield the seismic velocity structure of Ninetyeast Ridge and adjacent oceanic basins from the traveltime data (Fig. 6). First, we used a tomographic inversion to obtain a detailed image of the crustal properties. This method, however, only considers first arrivals. We therefore divided the transect into two profiles: the Ninetyeast Ridge edifice and the Indian Basin (profile 05 and western instruments of profile 06, called profile 05), and the Wharton Basin (eastern instruments
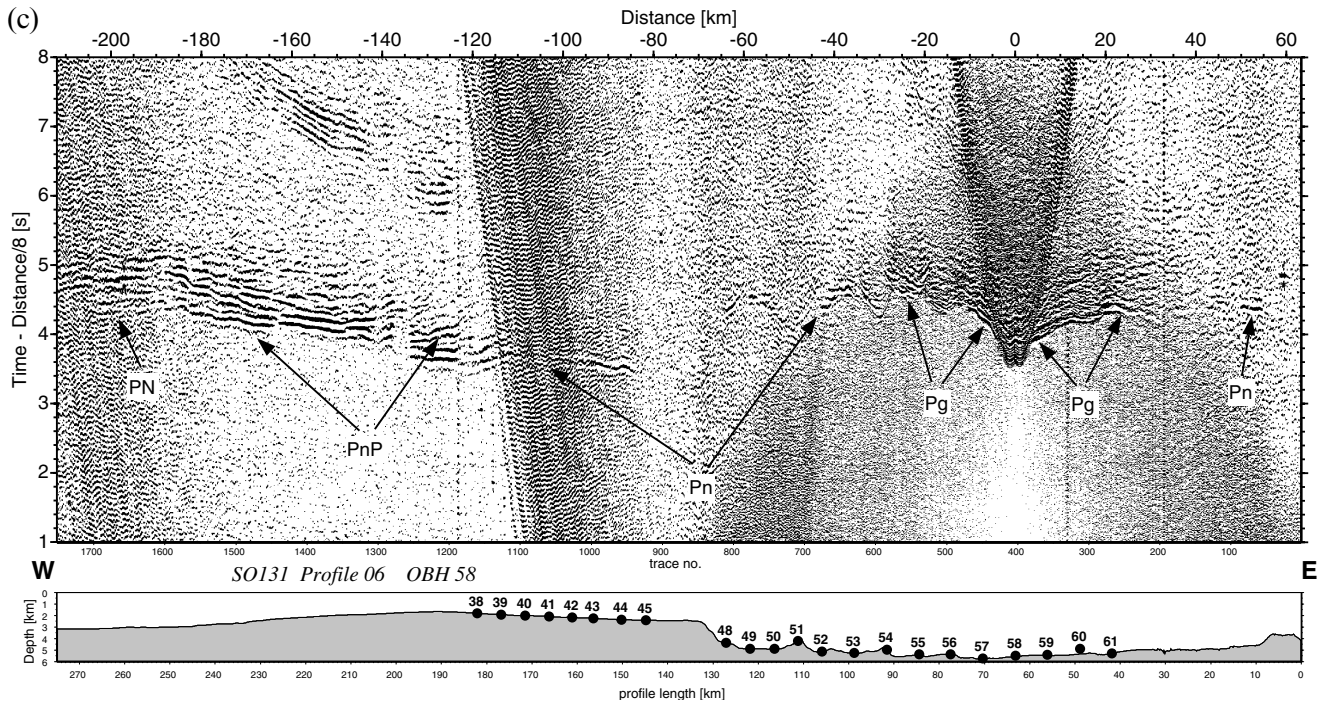
Figure 4. (*Continued.*)

of profile 06 and profile 31, called profile 31). This approach was reasonable because we observed in the Wharton Basin clear *Pg* and *Pn* arrivals, while instruments on the edifice recorded only *Pg* phases as first arrivals.

The second approach was chosen to take advantage of wide-angle reflection phases to reveal the crustal and upper mantle structure under Ninetyeast Ridge. To model the different mantle

reflection phases observed primarily on Ninetyeast Ridge and adjacent instruments, we used a 2-D ray tracing program.

4.1 Tomographic inversion of first arrivals

To assess the seismic velocity of the crustal rocks we applied a tomographic inversion method to first-arrival traveltimes
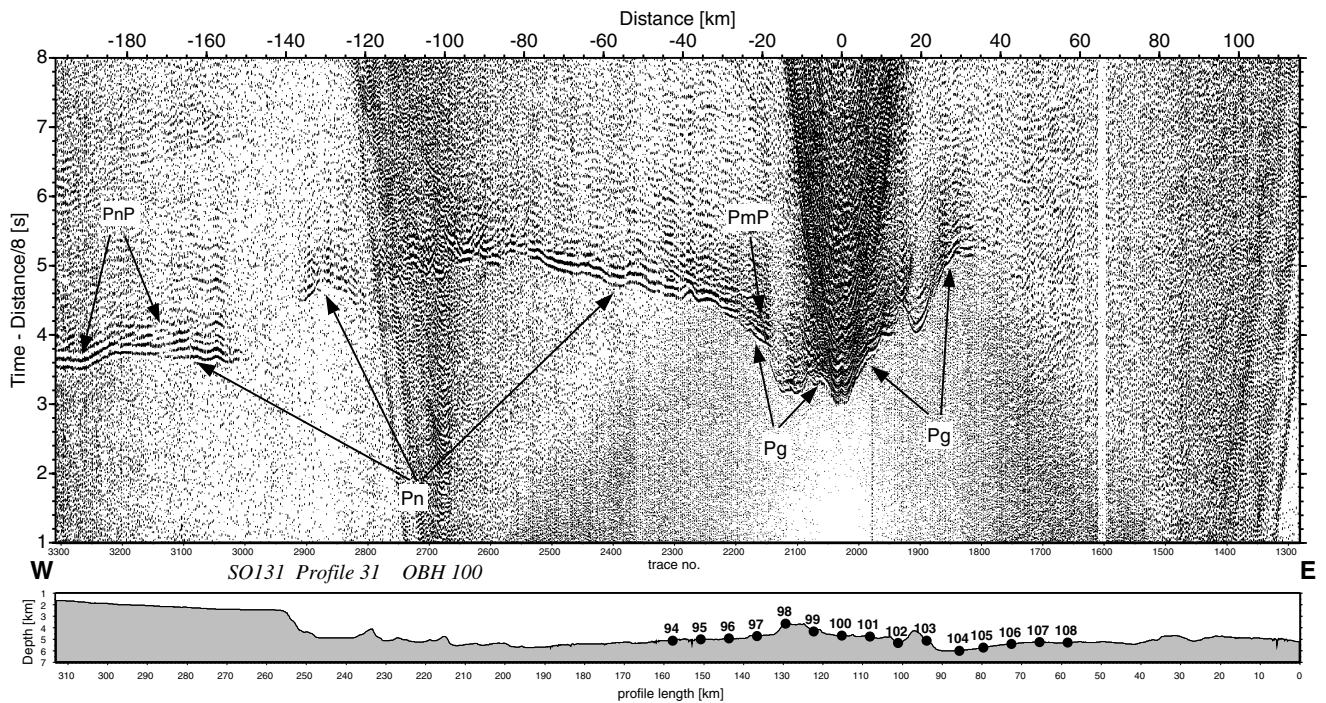

Figure 5. Hydrophone data from airgun shots over OBH 100 on profile 31. Data processing and phases as in Fig. 3.
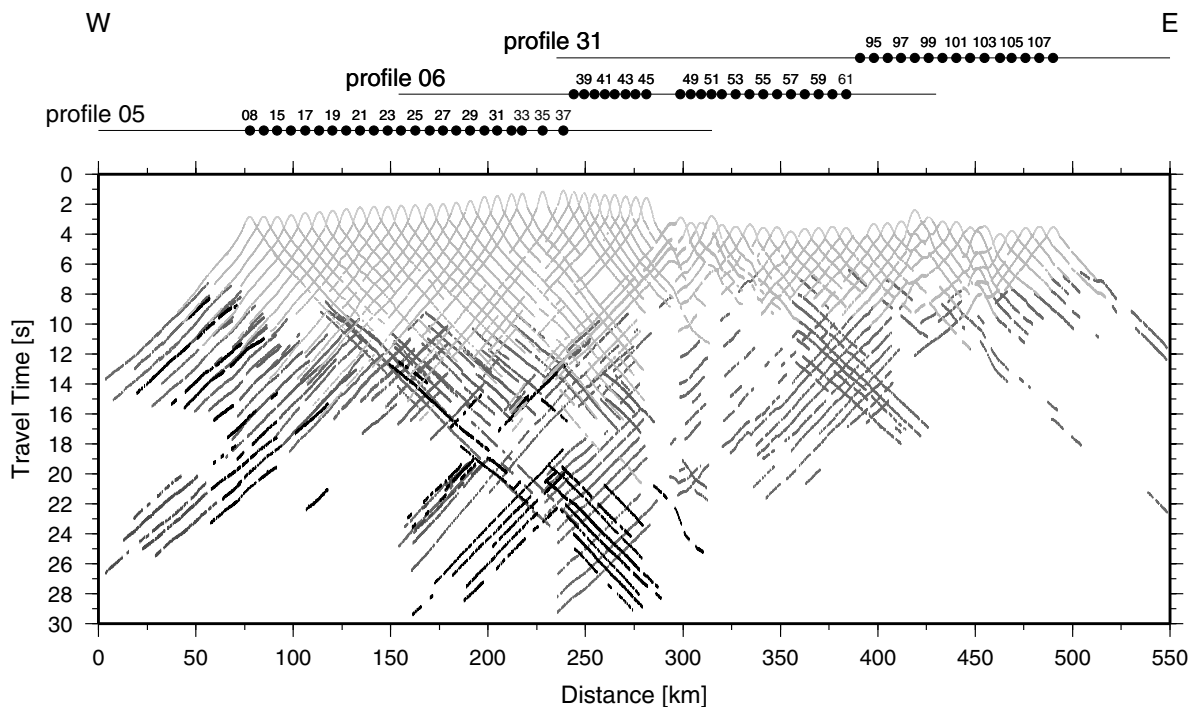
Figure 6. (Top) coverage and instruments available on profiles 05, 06 and 31, respectively. (Bottom) picked traveltimes used to reveal seismic velocities. Grey bars are *Pg* arrivals and the dark arrivals are from the crust–mantle boundary region and from the upper mantle.

which relies on traveltime computation using finite difference algorithms developed by Vidale (1988, 1990) and a non-linear inversion of arrival times for subsurface slowness based on a modification of a method introduced by Ammon & Vidale (1993). A detailed description and discussion of this approach is given elsewhere (Parson *et al.* 1996).

The starting velocity models for tomographic inversion are based on velocity–depth solutions obtained by forward modelling of traveltime data from OBH 8 and OBH 38. OBH 8 was located adjacent to Ninetyeast Ridge in the Indian Basin and was chosen to provide constraints on the structure of pre-existing oceanic crust, while OBH 38, located on the ridge, sampled the structure of the volcanic edifice. We used a 2-D ray tracing algorithm (Zelt & Smith 1992), although we only introduced 2-D features at the seafloor and the acoustic basement, where they are constrained by seismic reflection data. Deeper layers, however, had zero dip.

The inversion models were parametrized using horizontal and vertical cell widths of 0.25 km. For the traveltime calculations the same grid size was chosen and velocity models were obtained after 10 iterations. The numbers of arrivals used were 16 961 and 9776 for profiles 05 and 31, respectively. The inversion was carried out using a 'top-down' approach; that is, we used arrivals from the *n*th phase, inverted the data, added arrivals from the *n* + 1th phase and started the inversion again. For profile 05, root mean square (RMS) traveltime residuals for the starting model and final model were 0.16 and 0.07 s, respectively, for upper crustal arrivals and 0.12 and 0.05 s, respectively, for both upper and lower crustal arrivals. Generally, we were able to reach final RMS traveltime residuals reflecting the picking uncertainty; that is, for profile 31 we obtained RMS errors of 0.07, 0.08 and 0.12 s for upper crustal, lower crustal and *Pn* arrivals, respectively. The results for the inversion of the Ninetyeast Ridge edifice (profile 05) are shown in Fig. 7.

4.2 Forward modelling of wide-angle phases

A first velocity model was developed using constraints from seismic reflection data (Flueh & Reichert 1998; Flueh *et al.* 1999b) and a simplified crustal model derived from the final tomographic inversion grids. We modelled the traveltime data using the ray tracing code from Zelt & Smith (1992). The program allows an iterative damped least-squares inversion of traveltimes. This approach, however, is strongly dependent on the model parametrization. The dimension of the long line and the number of layers, along with the roughness of crustal interfaces, makes it difficult to set up a model not biased by the parametrization. Alternatively, it will be overparametrized. Moreover, our main goal was to obtain a general image which provided a reasonable structural model. Thus, we used a forward modelling approach to fit observed and calculated traveltimes within their error bounds.

The traveltimes were again calculated using a 'top-down' approach, modelling the velocity and depth to each layer before moving to the next. Each layer is defined by a series of boundary nodes along its upper surface and velocity nodes along its upper and lower surfaces. If an 'upper' layer is not sampled by rays, its thickness or velocity is adjusted, if necessary, to assist the fitting of traveltimes to other phases that transited the layer. However, the spacing of ocean bottom instruments provided an excellent coverage of upper and mid-crustal layering; thus we have a good 'static' for rays turning in the crust–mantle boundary region and within the upper mantle.

To assess the quality of modelling, we used the RMS traveltime, the number of observations and the χ^2 parameter. These parameters quantify the fit between the observed and computed arrival times (Zelt & Smith 1992). This analysis indicates errors of about ± 0.1 km s^{-1} for the *P*-wave velocities and suggests that the thickness of the layers is calculated with
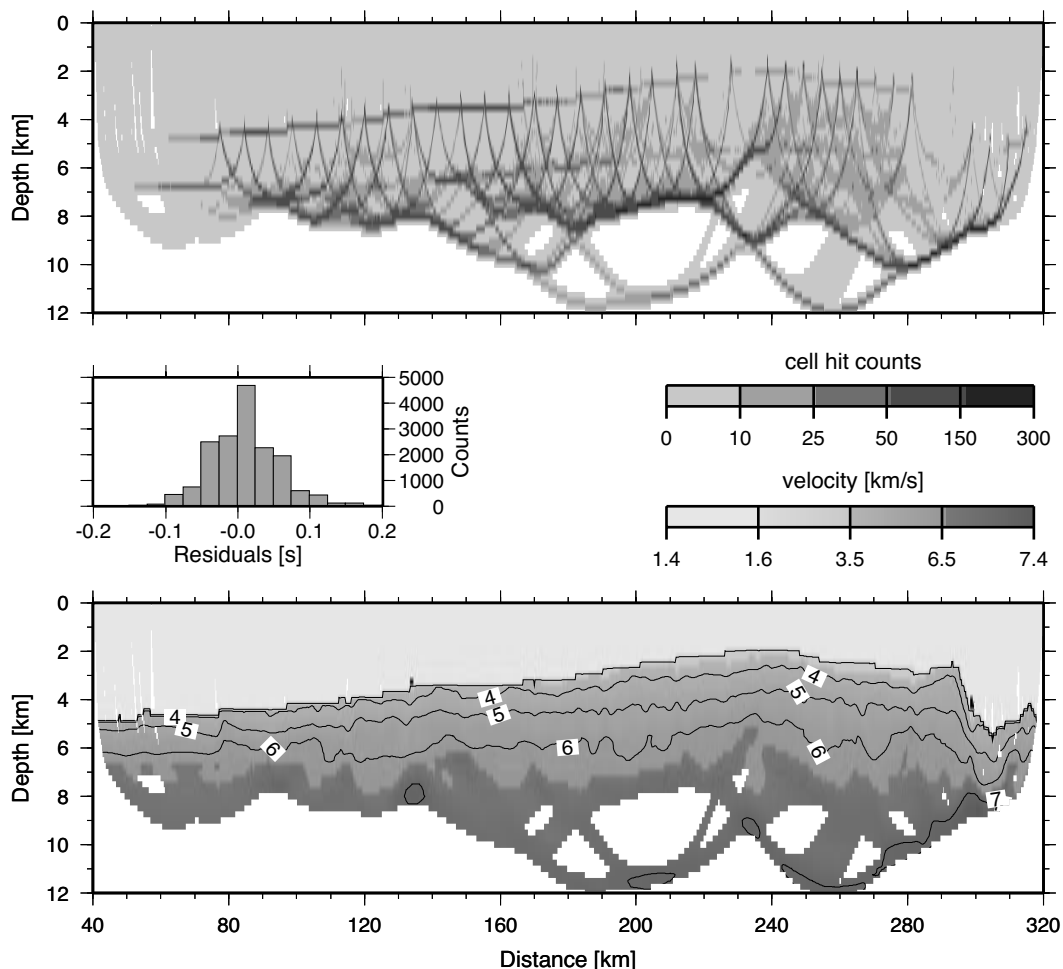
Figure 7. Results from the tomographic inversion of *Pg* arrivals from the Ninetyeast Ridge edifice, profile 05, showing coverage, statistics of traveltime residuals and velocity model (contours in km s^{-1}).

uncertainties of 10–15 per cent and ≈ 20 per cent for crustal and upper mantle layers, respectively.

Additional constraints have been placed on the velocity gradients by calculating synthetic seismograms for major crust and upper mantle arrivals. Using the code of Zelt & Ellis (1988), amplitudes were fitted subjectively, matching the principal variations in the seismic records. Like the ray-tracing modelling code, the calculation of synthetics was based on asymptotic ray theory.

5   RESULTS AND INTERPRETATION

In this section we will discuss the results from the tomographic inversion and from forward modelling of wide-angle phases in terms of a reference structure. We chose the structure revealed by the joint approach of White *et al.* (1992), which may represent typical oceanic crust.

5.1   Tomographic inversion of first arrivals

The main results from the tomographic inversion are shown in Figs 7 and 8 and indicate typical oceanic crust in the Wharton Basin (profile 31) and in the Indian Basin (the westernmost instruments on profile 05). The upper crustal section of oceanic

crust has, at its top, velocities of 3.9–4.3 km s^{-1} which increase rapidly with depth to values of 6.5 km s^{-1} at the base. These values are within the range of velocities associated with layer 2, and hence basaltic rocks emplaced by extrusive and intrusive volcanism (e.g. White *et al.* 1992; Grevemeyer & Weigel 1996). The layer 2/3 transition zone is marked by a decrease in the vertical velocity gradient. Within layer 3, velocities are between 6.7 and 7.2 km s^{-1}, thus indicating ultrabasic or mafic rocks, generally associated with layer 3 (e.g. White *et al.* 1992). Crustal thickness (where sampled) averages 6.5–7 km and is therefore in excellent agreement with the mean thickness of oceanic crust (White *et al.* 1992). It is, however, between 0.5 and 1 km thinner than crust created at the fast-spreading East Pacific Rise (White *et al.* 1992; Grevemeyer *et al.* 1998).

Approaching the edifice, the upper crustal thickness increases significantly, suggesting a thickening of the extrusive layer. In addition, velocities at the seafloor are lower when compared to values found for the adjacent oceanic bedrock. The lower velocities are indicative of lower densities and higher porosities and are due to eruptions at shallower depth (Peterson & Moore 1987) and higher lava cooling stresses (Bonatti & Harrison 1988). Moreover, drilling (Peirce *et al.* 1989) and an on-bottom seismic experiment (Grevemeyer *et al.* 1999) indicate a 100–200 m thick layer of volcaniclastic sediment. Such a thin layer, however, would not be detected with the set-up of our experiment.
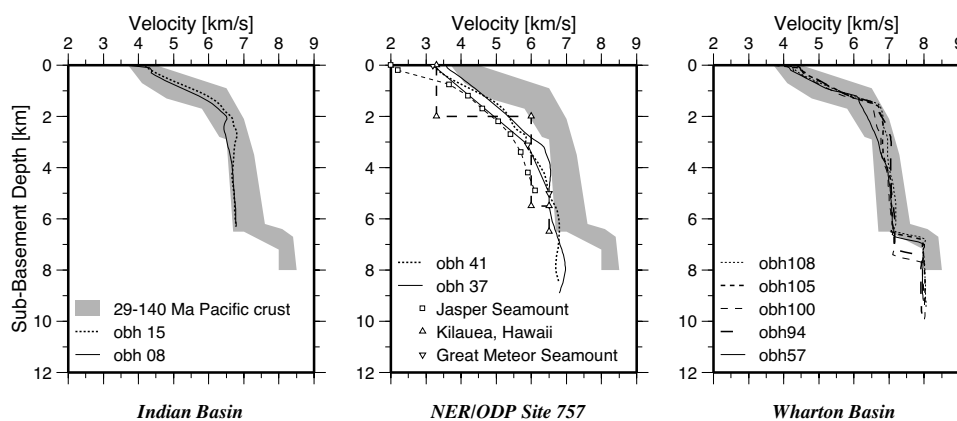
Figure 8. Summary of the results from the tomographic inversion of profile 05 [Indian Basin and Ninetyeast Ridge (NER) edifice] and profile 31 (Wharton Basin). The Pacific crust data for 29–140 Ma are from White *et al.* (1992); the Jasper seamount, Kilauea and Great Meteor seamount profiles are from Hammer *et al.* (1994); Klein (1981) and Weigel & Grevemeyer (1999), respectively.

Thus, in addition to the processes cited above, the inversion may average velocities of clastic material and of uppermost volcanic bedrock.

Within the edifice, the transition between basaltic and ultra-basic material occurs at about 3–4 km depth. At other seamounts or LIPs, this transition is detected at a similar depth, which may indicate common processes acting on and controlling the emplacement of LIPs. The crustal base, however, was not revealed by the tomographic inversion, but could be studied in detail by forward modelling of wide-angle reflections.

5.2 Forward modelling of deep crustal and mantle phases

Like the tomographic inversion, the modelling of crustal arrivals provided basically the same features. The excellent coverage of *Pg* arrivals (Fig. 7) provided the required 'static' to reveal deep crustal and upper mantle properties, that is, the quality of the whole data set is high enough to detect variations at the crust–mantle boundary region which are solely due to the geometry of layering and/or velocity variations (Fig. 9).

The pre-hotspot crust–mantle boundary is flexed or has moved downwards under the ridge, indicating the isostatic response of loading the seafloor. In addition, the pre-existing crust is heavily underplated by material with seismic velocities of 7.5–7.6 km s^{-1}. This body is up to 7 km thick; thus, crust is up to 24 km thick. It is important to note that underplating also occurs eastwards of Ninetyeast Ridge (Figs 9, 10 and 11), suggesting that some material was added to the crust after Ninetyeast Ridge was pulled apart from Broken Ridge. Previous studies have generally detected high-velocity lower crust (i.e. underplating) under seafloor with a positive depth anomaly (Watts *et al.* 1985; Caress *et al.* 1995; Charvis *et al.* 1999). The Wharton Basin to the east, however, did not provide any depth anomaly. Nevertheless, the maximum thickness was encountered under the edifice where the seafloor reached its minimum depth. The geometry of the underplating body is clearly constrained by *PmP* arrivals from its top and *Pm₂P* and *Pn* arrivals reflected at the crustal base and turning within the uppermost mantle, respectively (Fig. 9). This excellent coverage established the existence of high-velocity material resident under the Ninetyeast Ridge and therefore supports models of melt generation at LIPs (White & McKenzie 1989; Keleman & Holbrook 1995).

However, within the upper mantle an additional boundary was detected. Both wide-angle reflection (Figs 9d and 10c) and refracted arrivals support this boundary and indicate velocities increasing from 8.2 to 8.4 km s^{-1} across the interface. Like the underplating body, this boundary was only detected beneath the edifice and its depth is not constrained under the Wharton basin to the east. Therefore, the feature might be closely related to hotspot volcanism. Similar features have been detected elsewhere, but have never been interpreted satisfyingly (Gallart *et al.* 1999; Ye *et al.* 1999), although a velocity of 8.4 km s^{-1} may indicate depleted mantle material or anisotropy (LADLE study group 1983; Smallwood *et al.* 1999).

The final velocity model presents an average model to fit the traveltimes within their error bounds. However, the model also produced the principal variations in amplitudes of the main refraction and wide-angle reflection branches (Fig. 10); that is, (i) the calculated synthetic seismograms show the profound variations in amplitudes of the *Pg* phases, indicating a high-gradient upper crust and a moderate-gradient mid to lower crust (Figs 10a–c), (ii) the synthetic seismograms confirm the observation that the *PmP* phase is generally much stronger than the *Pm₂P* phase, explaining why the *PmP* arrivals are more prominent in seismic record sections (Figs 10a and c), and (iii) the modelled amplitude pattern provides the high-amplitude *PnP* and associated refraction branch *P_N* at offsets of more than 90–100 km (Figs 10c and d). Although the model (Figs 11a and b) may not account for all amplitude variations exhibited, it will present a reasonably good approximation of the main structural features of the hotspot track.

6 DISCUSSION AND CONCLUSIONS

6.1 Crustal architecture

Crustal structure has important implications for the evaluation of the extrusive and clastic processes acting on LIPs. The nature of eruptive, clastic and depositional mechanisms change drastically during growth of a seamount. At least three major depositional sites develop: summit, flank and apron facies (Staudigel & Schmincke 1984). Non-explosive and extrusive processes prevail in the deep-water stage, dominantly producing pillow basalts (≈ 75 per cent). The shallow water or shoaling
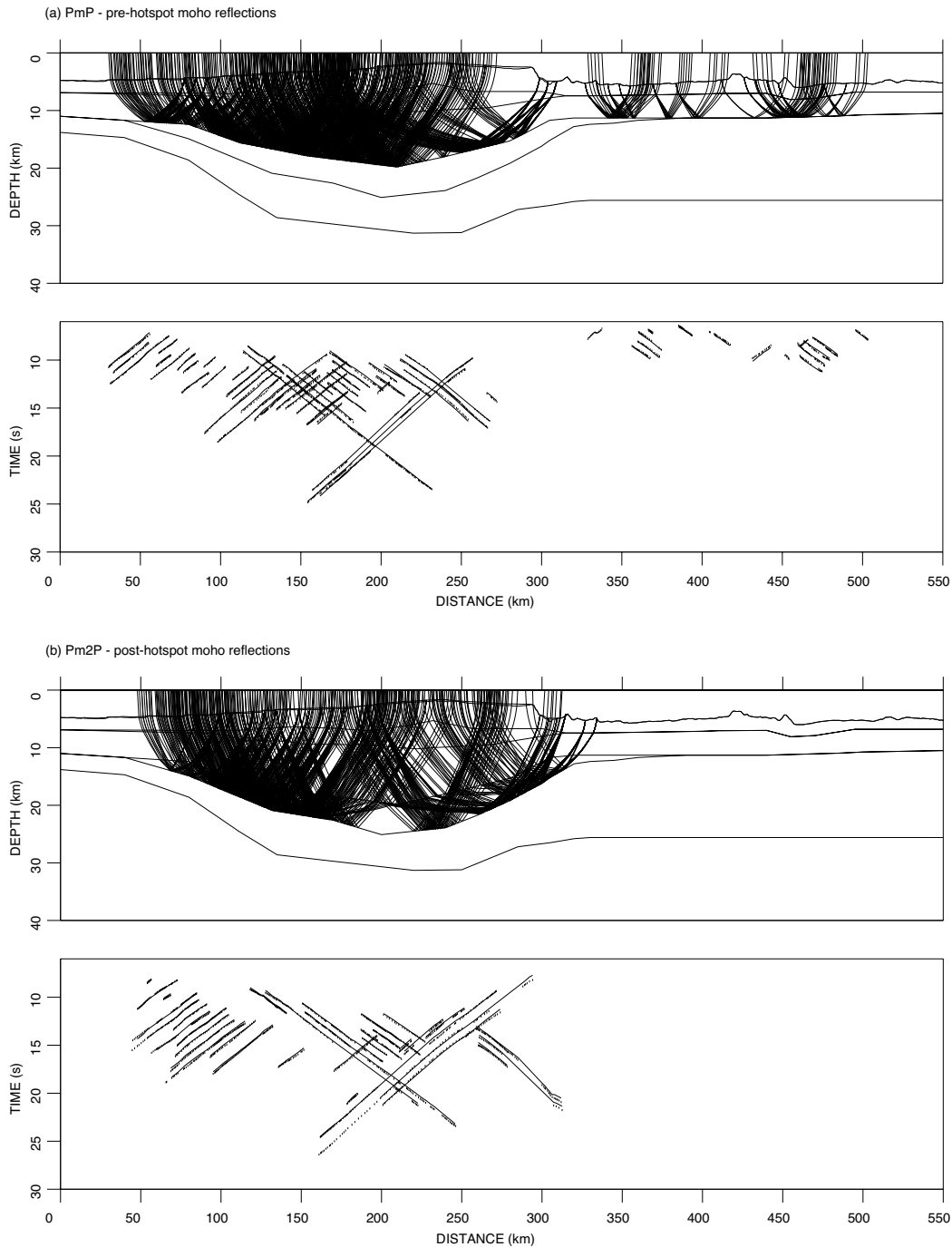
Figure 9. Ray tracing results from forward modelling of deep crustal and upper mantle arrivals. The top panels show the ray coverage and the bottom panels the observed (bars) and calculated traveltimes (solid lines). (a) *PmP*; (b) *Pm₂P*; (c) *Pn*; and (d) *PnP* arrivals.

stage is reached when a seamount top reaches the critical depth for a drastic increase in exsolution of magmatic volatiles, resulting in the formation of mainly clastic rocks (≈ 70 per cent). The accumulation of large volumes of clastic material in the summit region and upper flanks, and their potential for slumping and re-sedimentation generates debris flows on the flanks and aprons (e.g. Moore *et al.* 1989; Rees *et al.* 1994; Watts & Masson 1995). Some of the individual debris avalanches are 100–200 km long and 1000–5000 km³ in volume (Moore *et al.* 1989; Watts & Masson 1995). Apron sediments

often extent out to several hundreds of kilometres from the island (Filmer *et al.* 1994; Wolfe *et al.* 1994). On the summit and flanks, clastic sediments and rocks show seismically low velocities of 2.8–3.2 km s^{-1} (Hill & Zucca 1987), but can also reach velocities of 4.0–5.0 km s^{-1} in the deep portions of the moat (Rees *et al.* 1994; Filmer *et al.* 1994; Wolfe *et al.* 1994). These values fall into the range of uppermost layer 2 velocities of mature oceanic crust (Grevemeyer & Weigel 1996). There-fore, seismic refraction studies and hence first-arrival tomo-graphy may not resolve the boundary between clastic fill in
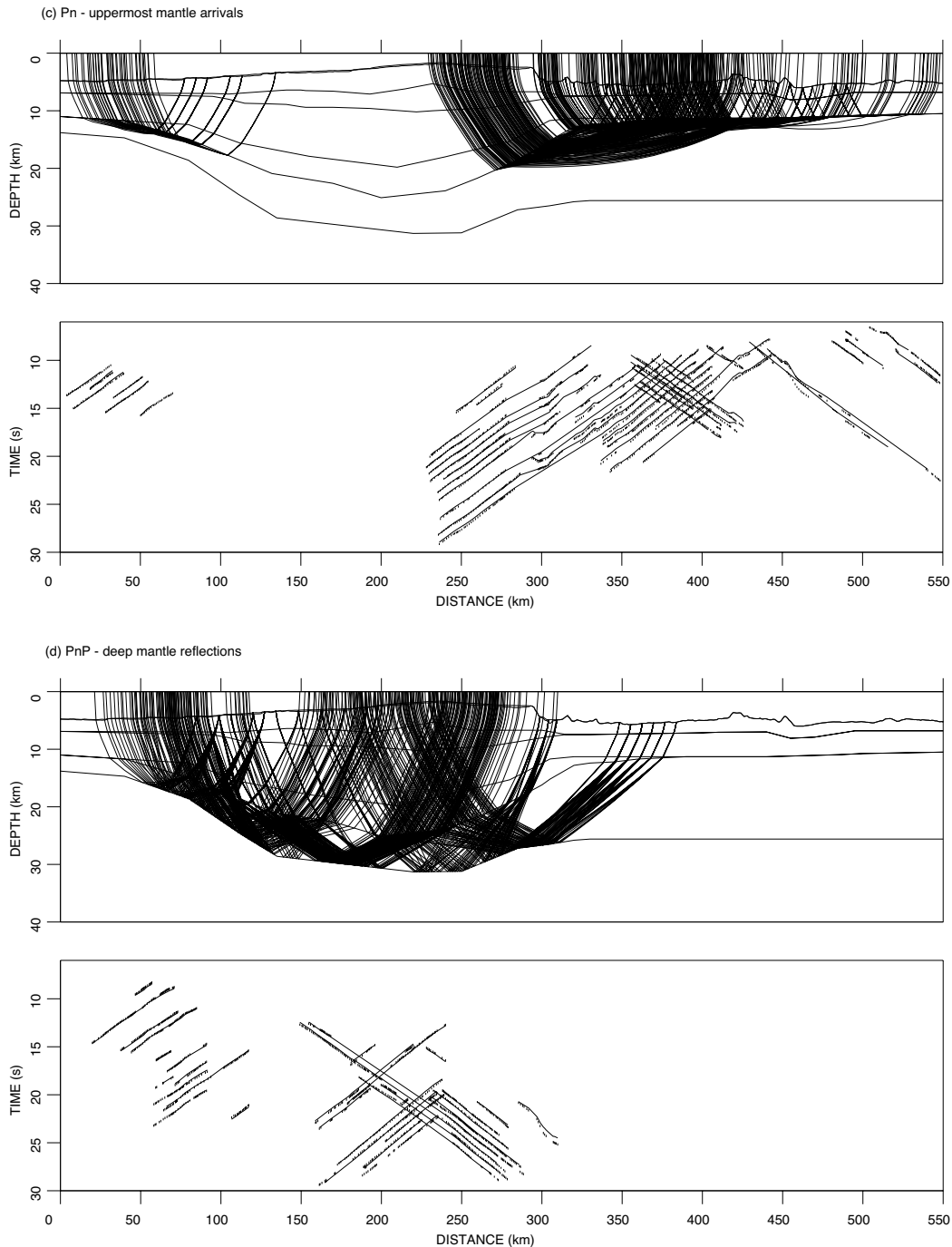
(c) Pn - uppermost mantle arrivals

(d) PnP - deep mantle reflections

Figure 9. (*Continued.*)

sediments and volcanic bedrock. In this case, final velocity models provide an unrealistically thick layer 2 (Weigel & Grevemeyer 1999), because both extruded and clastic rocks contribute to the seismically defined upper crustal layer.

To provide a structural comparison between apron, flank and summit we use the correlation between sub-basement velocity profiles from our study and other seamounts (e.g. Klein 1981; Hammer *et al.* 1994; Weigel & Grevemeyer 1999) and oceanic crust, as determined by White *et al.* (1992). The results are shown in Fig. 8. For the summit and flanks only (not shown), rock with velocities within the range of extrusive or clastic

material built up a section thicker than layer 2 of oceanic crust. The transition to gabbroic rocks occurs at 3–4 km depth. Compared to other seamounts, a similar transition depth was detected, suggesting that most seamounts are built up by similar processes. Reasonably close to the edifice, properties typical of layer 2 have been found. This has important implications for the architecture and formation of the edifice. Most importantly, clastic processes have not been abundant, suggesting that most parts of the upper crust are composed of extruded basalts. Therefore, it seems reasonable to suggest that Ninetyeast Ridge never reached, or remained only for a short
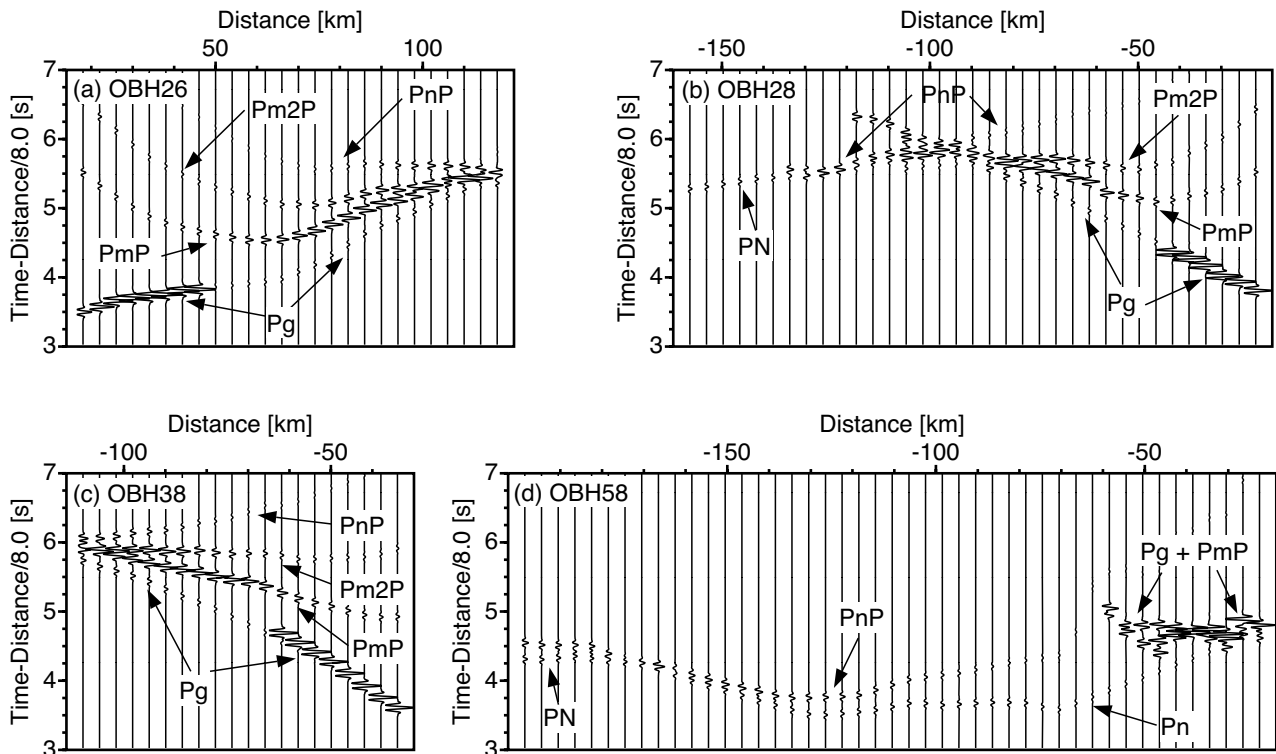
Figure 10. Examples of amplitude modelling for major crustal and upper mantle arrivals. (a) OBH 26, (b) OBH 28, (c) OBH 38 and (d) OBH 58. Recorded sections are shown in Figs 3(c) and (d) and 4(a) and (c), respectively.

time interval in, the shoaling stage. This idea is supported by the morphology of the ridge and by drilling results. A multibeam sonar survey (Flueh & Reichert 1998; Flueh *et al.* 1998) did not provide any evidence for a guyot stage, which would indicate that a volcanic island was eroded at the wave-base. In contrast, the survey detected several intact small-sized volcanic cones near the summit, indicating that these features have been emplaced in shallow to mid-depth water. Otherwise, they would have been eroded.

At ODP site 757, the eruptive centre was at or near sea level (Peirce *et al.* 1989). Site 758, however, provided only pillow basalts erupted in deep water. Site 757 was drilled into a sequence of dipping reflectors (Flueh *et al.* 1999a,b), generally associated with a shallow-water emplacement of extrusives (e.g. Hinz 1981; Mutter *et al.* 1982; Planke & Eldholm 1994). This sequence is well preserved, suggesting a rapid subsidence after its emplacement, which is consistent with the subsidence history derived from ODP drilling results (Peirce *et al.* 1989; Grevemeyer & Flueh 2000). Thus, there are several lines of evidence which suggest that most parts of Ninetyeast Ridge never reached sea level, or if they did, the edifices subsided rapidly, providing a structure primarily constructed from extruded basalts. Therefore, in contrast to other hotspot regions such as the Hawaiian, Marquesas or Canary islands (e.g. Moore *et al.* 1989; Wolfe *et al.* 1994; Watts & Masson 1995), the Ninetyeast Ridge is not surrounded by a large clastic apron.

Fig. 12 shows the interpretation of the velocity model (Fig. 11). Because we could not identify energy coming from the top of the pre-hotspot crust, we assumed that the thickness of crust adjacent to the ridge could be used to characterize pre-hotspot crust. Based on this assumption we estimated the location of the top of the crust by shifting the seismically

detected pre-hotspot crust–mantle boundary upwards by 6.5 km. The resulting structure suggests that in addition to the high-gradient basaltic section, high-velocity and moderate-gradient mafic material has also been added to form the edifice. Furthermore, we believe that the pre-hotspot crust is heavily intruded, because we could not trace a seismic boundary separating the volcanic edifice from the top of the pre-hotspot crust. Based on these assumptions, we roughly estimate, within the error bounds of refraction seismology, that basaltic and mafic rocks make up about the same volume of the edifice.

6.2 Hotspot-related underplating

From the seismic detection of lower crustal velocities exceeding 7.1–7.2 km s^{-1} it has been proposed that a significant proportion of the products of hotspot volcanism was formed from melt trapped or intruded near the base of the crust (White & McKenzie 1989; Holbrook 1995). The high-magnesium basalts generated from abnormally hot mantle typically exhibit high densities and hence velocities when they crystallize (White & McKenzie 1989; Keleman & Holbrook 1995). The base of the crust forms a marked density contrast, so it is likely that melts generated at depth will accumulate near the base of the crust, where they either underplate the crust or intrude it as sills. High-velocity lower crust is observed at rifted volcanic margins (White *et al.* 1987; Eldholm & Grue 1994) or under seamounts (e.g. Watts *et al.* 1985; ten Brink & Brocher 1987; Caress *et al.* 1995; Charvis *et al.* 1999). Other hotspot provinces, however, did not provide evidence for underplating (Operto & Charvis 1996; Watts *et al.* 1997).

Compared to all previous surveys over hotspot provinces, our investigation provided a much denser spacing of ocean bottom
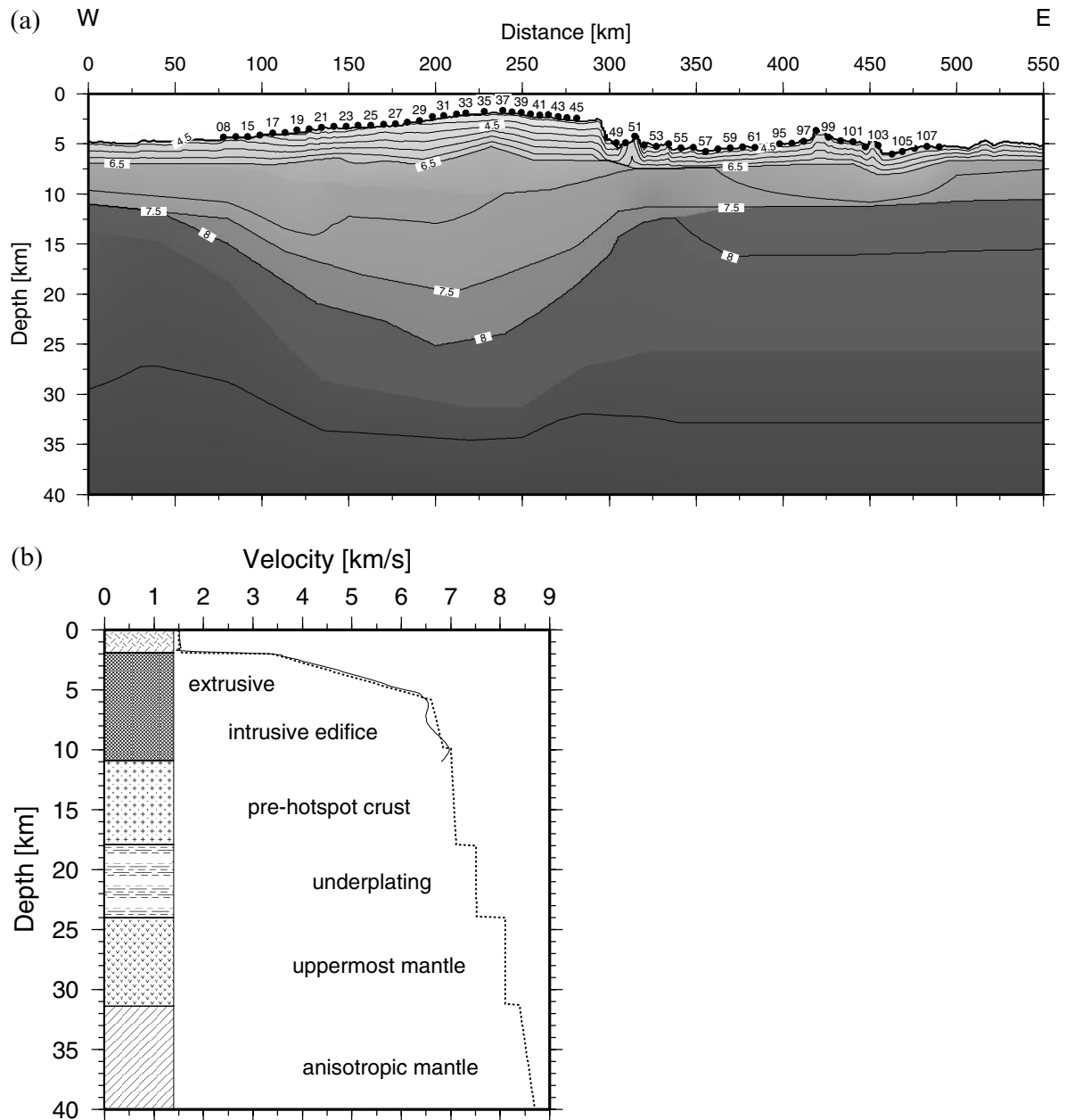
Figure 11. (a) Final velocity model used to calculate traveltimes shown in Fig. 9. Contour interval is 0.5 km s^{-1}. ODP site 757 is coincident with OBH 37. (b) Velocity–depth solution and interpretation of layering at the location of ODP site 757, i.e. at 238 km (OBH 37). The solid line is from the tomographic inversion and the broken line from the forward modelling approach.

recorders. Moreover, most of the other studies investigated hotspot islands, while we surveyed a submerged feature. The study of an island generally suffers from missing shots on the island itself, or if they exist, from large shot spacing of land shots. An experiment conducted over a submarine structure allows continuous coverage along a profile. Therefore, our survey provides a unique data set to investigate upper mantle properties over an ancient hotspot. From the 60 instruments we picked 5295 *PmP* arrivals from the pre-hotspot crust–mantle boundary and 3935 *Pm$_2$P* arrivals from the post-hotspot Moho. This coverage establishes that crustal underplating presents an integral part of hotspot volcanism at intraplate islands or LIPs (e.g. Holbrook 1995). Moreover, the occurrence of under-

plated material under the Wharton Basin (that is, to the east of the transform boundary along which Ninetyeast Ridge was sheared off Broken Ridge) has important implications for the timing of late-stage magmatism. This fact clearly indicates that at least some underplating occurred after the emplacement of the Ninetyeast Ridge and after the edifice was pulled apart from Broken Ridge. This could explain the anomalous sub-sidence of Ninetyeast Ridge discussed by Grevemeyer & Flueh (2000). Unfortunately, the coverage with magnetic survey lines in the vicinity of Ninetyeast Ridge is rather poor; thus the offset along the fracture zone is difficult to quantify. Nevertheless, the plate tectonic reconstruction of Royer *et al.* (1991) and the digital age map of Müller *et al.* (1997) provide an initial
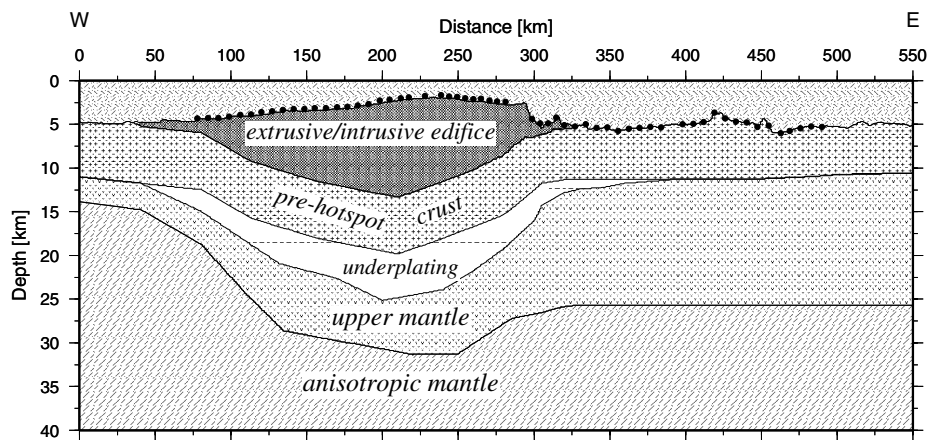
W   Distance [km]   E

Figure 12. Interpretation of the velocity model shown in Fig. 11(a). The top of pre-hotspot crust was generated by an upward shift of the seismically defined pre-hotspot crust–mantle boundary by 6.5 km, the mean crustal thickness of oceanic crust found in adjacent ocean basins. All other layers are from boundaries derived by seismic inversion and modelling (see Figs 7, 8 and 9).

assessment and may suggest that underplating occurred for 15–20 Myr. This has important implications for the hotspot flow and indicates flow of hotspot material along the fossil trail.

6.3   Upper mantle properties

A striking feature in our record sections is the *PnP* and P_N phases, associated with a high-velocity layer (8.4–8.6 km s^{-1}) within the uppermost mantle. However, its geodynamic implications are difficult to explain. Similar reflections have been observed at La Réunion (Gallart *et al.* 1999), Gran Canary (Ye *et al.* 1999) and Iceland (Smallwood *et al.* 1999). Long-range seismic profiles in the Atlantic ocean detected a stratified upper mantle and provided quite similar arrivals and velocities at similar depth intervals (e.g. LADLE study group 1983; Pavlenkova 1996). Thus, it might be reasonable to suggest that its occurrence is simply a fact of profile lengths, that is, most seismic refraction lines did not reach the required shot–receiver offsets. On the other hand, our survey only imaged the layer under the edifice, which may suggest a close relationship between hotspot volcanism and its formation.

We believe that the most likely interpretation for this layer is given by the LADLE study group (1983) and Smallwood *et al.* (1999). They suggested either that the layer is composed of eclogite, formed by basaltic melt freezing near the base of lithosphere, or that the velocity contrast is caused by anisotropy of olivines, perhaps in conjunction with the spinel–garnet peridotite phase change. The preferred orientation could be due to the flow of hotspot material rising over the hotspot and spreading away under the lithosphere. Both models can explain why the boundary is shallower under the Indian Basin than under the Wharton Basin, which might be a simple interaction between the deformation of lithosphere due to surface loading, plate flexure and the age of lithosphere, which is younger under the Indian Basin to the west of Ninetyeast Ridge and hence thermally thinner. Under Iceland, the lack of a conspicuous gravity signal corresponding to a dense body associated with the *PnP* (or *PxP* as it is called by Smallwood *et al.*) reflection favours a model incorporating upper mantle anisotropy (Smallwood *et al.* 1999). For Ninetyeast Ridge the cross-spectral analysis of gravity and bathymetric data provided an isostatic model indicating both surface loading of a thin elastic lithosphere and

buoyant loading at its base (Grevemeyer & Flueh 2000). This model could also explain the anomalous low subsidence history of Ninetyeast Ridge. High-density eclogite frozen at the base of the lithosphere would contradict this model.

6.4   Model of Ninetyeast Ridge magmatism

It is known from plate tectonic reconstructions (Royer *et al.* 1991) and from the tholeiitic, iron-rich and voluminous character of basalts (Saunders *et al.* 1991) that the Ninetyeast Ridge was emplaced on or near a mid-ocean spreading centre. Drilling indicates that the ridge was constructed by discrete, subaerial and/or shallow-water volcanic centres (Peirce *et al.* 1989). The locations of volcanic centres on the ridge formed a succession from deep-water submarine flows (site 758) to phreatic eruptions to subaerial flows (site 757), followed by a second phase of phreatic eruption as the mature volcano subsided when moving away from the hotspot (site 757). However, at any time during the history of Ninetyeast Ridge, different types of volcanic activity were occurring simultaneously on different parts of the ridge. Although seismic reflection profiling (Flueh *et al.* 1999a,b) supports subaerial or shallow-water activity by revealing wedges of dipping seismic reflections, typical of volcanic rifted margins (Hinz 1981; Mutter *et al.* 1982), the same data suggest that the ridge sampled at site 757 did not remain for a long time at or near the wave base. This conclusion seems reasonable because the dipping reflector sequences are well preserved and also volcanic cones detected in multi-beam sonar data have not been affected by erosion. Additionally, as discussed above, the seismic refraction data provided no evidence for a large clastic apron, which would be expected if a seamount reaches a critical depth or becomes a volcanic island (Staudigel & Schmincke 1984). We believe that this is because the Ninetyeast Ridge was emplaced on a young and rapidly drifting plate. First, young lithosphere is elastically thin and therefore may account for rapid initial subsidence (Grevemeyer & Flueh 2000) after the major shield-building phase. Second, because the plate was moving fast (Royer *et al.* 1991), the volcanic centre was removed early from its heat source. Consequently, the edifice is primarily built up of extrusives and intrusives and has only a small clastic apron.

The occurrence of small volcanic cones near the summit of Ninetyeast Ridge suggests that these features formed while the ridge was already subsiding. Therefore, they are related to late-stage volcanism (Flueh *et al.* 1998). The escarpment to the east was formed when the ridge was pulled apart from Broken Ridge (Royer *et al.* 1991). The occurrence of underplated material to the east of the escarpment suggests that underplating of Ninetyeast Ridge took place over a long time after the shield-building stage. Underplating is associated with buoyant forces acting on the lithosphere. These forces could explain the low subsidence of Ninetyeast Ridge (Grevemeyer & Flueh 2000). Ito & Clift (1998) suggest that for some Pacific plateaus, prolonged crustal growth in the form of underplating may have occurred over a time of ≈ 30 Myr. The age offset across the fracture zone separating Ninetyeast Ridge from the Wharton Basin is only poorly constrained. An initial assessment based on plate tectonic reconstructions (Royer *et al.* 1991; Müller *et al.* 1997) provided an age of ≈ 5–10 Ma and thus possibly about 15–20 Myr of prolonged crustal growth by underplating. A detailed discussion of the implications of magmatic underplating on the subsidence and isostasy and its timing will be given elsewhere (Grevemeyer & Flueh 2000).

A major conclusion of our survey is that nearly the same volume of magmatic material that erupted on the seafloor or intruded into the edifice has been added to the crust to form an underplated layer. Assuming an Airy-type isostatic compensation mode of Ninetyeast Ridge, Schubert & Sandwell (1989) estimated volumes of 1.9×10^6 and 8.4×10^6 km^3 for the edifice and crustal root, respectively. In terms of our estimates derived from the seismic constraints, we calculate a volume of 8.2×10^6 km^3 for the edifice and fill-in and 5.4×10^6 km^3 for the subcrustal plutonic complex, that is, the ratio between the mafic/ultramafic underplate and extrusive/intrusive rocks is about 0.7. Differences between the Schubert & Sandwell assessment and our calculations are related to their assumption that the edifice is Airy-type compensated. Our data indicate an elastic plate which was bent downwards by loading it, thus fill-in provided an additional amount of material emplaced. Fill-in sediments and flows, however, are not considered by assuming an Airy-type compensation. In addition, underplating provided buoyant forces. Therefore, both the elastic properties of the crust and buoyancy compensate the load. Consequently, the volume of the surface load (edifice) is larger and the volume of the crustal root is smaller. Nonetheless, melt trapped at the crustal base forming subcrustal plutonic complexes presents an integral part of LIPs and these have to be considered by estimating the volume of hotspot magmatism (Holbrook 1995).

At the Marquesas Islands, however, Caress *et al.* (1995) detected a ratio of material forming the underplate and the edifice of about 1.9, thus about three times the volume sampled during our survey. Under La Réunion, in contrast, a volume of underplated material similar to our estimates was detected (Charvis *et al.* 1999; Gallart *et al.* 1999). Underplating may occur over millions of years after the initial shield-building phase (Ito & Clift 1998). With respect to the hotspot reference frame, the Indian plate and hence Ninetyeast Ridge was moving rapidly northwards. Thus, it might be reasonable to suggest that Ninetyeast Ridge was removed earlier from its heat and magma source than the Marquesas Island; consequently, prolonged crust growth by underplating ceased earlier. This conclusions would suggest that crustal underplating is related to late-stage volcanism, which, indeed, is supported by material found east-ward of Ninetyeast Ridge and subsidence studies of Pacific plateaus (Ito & Clift 1998) and Ninetyeast Ridge (Grevemeyer & Flueh 2000).

REFERENCES

Ammon, C.J. & Vidale, J.E., 1993. Tomography without rays, *Bull. seism. Soc. Am.,* **83,** 509–528.

Bialas, J. & Flueh, E.R., 1999. Ocean bottom seismometers, *Sea Technol.,* **40,** 41–46.

Bonatti, E. & Harrison, C.G.A., 1988. Eruption styles of basalts in oceanic spreading ridges and seamounts, *J. geophys Res.,* **93,** 2967–2980.

ten Brink, U.S. & Brocher, T.M., 1987. Multichannel seismic evidence for a subcrustal complex under Oahu and a model for Hawaiian volcanism, *J. geophys. Res.,* **92,** 13 687–13 707.

Campbell, I.H. & Griffiths, R.W., 1990. Implications of mantle plume structure for the evolution of basalts, *Earth. planet. Sci. Lett.,* **99,** 79–93.

Caress, D.W., McNutt, M.K., Detrick, R.S. & Mutter, J.C., 1995. Seismic imaging of hotspot-related crustal underplating beneath the Marquesas islands, *Nature,* **373,** 600–603.

Charvis, P. *et al.,* 1999. Spatial distribution of hotspot material added to the lithosphere under La Réunion, from wide-angle data, *J. geophys. Res.,* **104,** 2875–2893.

Coffin, M.F. & Eldholm, O., 1992. Volcanism and continental break-up: a global compilation of large igneous provinces, in *Magmatism and the Causes of Continental Break-Up,* eds Storey, B.C., Alabaster, T. & Pankhurst, R.J., *Geol. Soc. Spec. Publ.,* **68,** 17–30

Coffin, M.F. & Eldholm, O., 1994. Large igneous provinces: crustal structure, dimensions, and external consequences, *Rev. Geophys.,* **32,** 1–36.

Duncan, R.A., 1991. Age distribution of volcanism along aseismic ridges in the eastern Indian ocean, *Proc. ODP Init. Repts,* **121,** 507–517.

Duncan, R.A. & Richards, M.A., 1991. Hotspots, mantle plumes, flood basalts and true polar wander, *Rev. Geophys.,* **29,** 31–50.

Eldholm, O. & Grue, K., 1994. North Atlantic volcanic margins: dimensions and production rates, *J. geophys. Res.,* **99,** 2955–2968.

Filmer, P.E., McNutt, M.K., Webb, H.F. & Dixon, D.J., 1994. Volcanism and archipelagic aprons in the Marquesas and Hawaiian islands, *Mar. geophys. Res.,* **16,** 385–406.

Flueh, E.R. & Bialas, J., 1996. A digital, high data capacity ocean bottom recorder for seismic investigations, *Int. Underwater Systems Design,* **18,** 18–20.

Flueh, E.R. & Reichert, C., eds, 1998. Cruise Report SO131, SINUS—Seismic investigations at the Ninetyeast Ridge observatory using SONNE and JOIDES RESOLUTION during ODP leg 179, *GEOMAR Rept,* **72,** 337.

Flueh, E.R., Klaeschen, D., Weinrebe, W. & Reichert, C., 1998. Investigation of small submarine volcanic cones at Ninetyeast Ridge by high resolution seismic investigations and bathymetry, *EOS, Trans. Am. geophys. Un.,* **79,** 872.

Flueh, E.R., Grevemeyer, I. & Reichert, C., 1999a. Ocean site survey reveals anatomy of a hotspot track, *EOS, Trans. Am. geophys. Un.,* **80,** 77.

Flueh, E.R., Grevemeyer, I. & Reichert, C., 1999b. Investigating the crustal framework at the NERO Hole 1107A, Leg 179, *JOIDES J.,* **25,** 14–16.

Gallart, J., Driad, L., Chauris, P., Sapin, M., Hirn, A., Diaz, J., de Voight, B. & Spachpazi, M., 1999. Perturbation to the lithosphere along the hotspot track of La Réunion from an offshore–onshore seismic transect, *J. geophys. Res.,* **104,** 2895–2908.

Grevemeyer, I. & Flueh, E.R., 2000. Crustal-underplating and its implications for subsidence and state of isostasy along the Ninetyeast Ridge hotspot trail, *Geophys. J. Int.,* **142,** 643–649.

Grevemeyer, I. & Weigel, W., 1996. Seismic velocities of the uppermost igneous crust versus age, *Geophys. J. Int.,* **124,** 631–635.

Grevemeyer, I., Weigel, W. & Jennrich, C., 1998. Seismic structure and crustal ageing at 14°S on the East Pacific Rise, *Geophys. J. Int.,* **135,** 573–584.

Grevemeyer, I., Flueh, E.R., Herber, R. & Villinger, H., 1999. Constraints on the shallow seismic structure at Ocean Drilling Program Site 1107, Ninetyeast Ridge, from implosive bottom sources and airgun shots, *Geophys. Res. Lett.,* **26,** 907–910.

Hammer, P.T.C., Dorman, L.M., Hildebrand, J.A. & Cornuelle, B.D., 1994. Jasper seamount: seafloor seismic refraction tomography, *J. geophys. Res.,* **99,** 6731–6752.

Hill, D.P. & Zucca, J.J., 1987. Geophysical constraints on the structure of Kilauea and Mauna Loa volcanoes and some implications for seismomagmatic processes, in *Volcanism in Hawaii,* eds Decker, R.W., Wright, T.L. & Stauffer, P.H., *USGS Prof. Paper,* **1350,** 903–917.

Hinz, K., 1981. A hypothesis on terrestrial catastrophes: wedges of very thick oceanward dipping layers beneath passive margins—their origin and paleoenvironmental significance, *Geol. Jahrb.,* **E22,** 3–28.

Holbrook, W.S., 1995. Underplating over hotspots, *Nature,* **373,** 559.

Ito, G. & Clift, P.D., 1998. Subsidence and growth of Pacific Cretaceous plateaus, *Earth planet. Sci. Lett.,* **161,** 85–100.

Keleman, P.B. & Holbrook, W.S., 1995. Origin of thick, high-velocity igneous crust along the U.S, East Coast margin, *J. geophys. Res.,* **100,** 10 077–10 094.

Kent, W., Saunders, A.D., Kempton, P.D. & Ghose, N.C., 1997. Rajmahal basalts, eastern India: mantle source and melt distribution at a volcanic rifted margin, in *Large Igneous Provinces: Continental, Oceanic, and Planetary Flood Volcanism,* eds Mahoney, J.J. & Coffin, M.F., *Geophys. Monograph,* **100,** 145–182.

Klein, E.W., 1981. A linear gradient model for south Hawaii, *Bull. seism. Soc. Am.,* **71,** 1503–1510.

LADLE Study Group, 1983. A lithospheric seismic refraction profile in the western North Atlantic ocean, *Geophys. J. R. astr. Soc.,* **75,** 23–69.

Larson, R.L., 1991. Geological consequences of superplumes, *Geology,* **19,** 963–966.

Mahoney, J.J., Macdougall, J.D., Lugmair, G.W. & Gopalan, K., 1983. Kerguelen hotspot source for Rajmahal traps and Ninetyeast Ridge?, *Nature,* **303,** 385–389.

Moore, J.G., Clague, D.A., Holcomb, R.T., Lipman, P.W., Normark, W.R. & Torresan, M.E., 1989. Prodigious submarine landslides on the Hawaiian Ridge, *J. geophys. Res.,* **94,** 17 465–17 484.

Morgan, W.J., 1971. Convection plumes in the lower mantle, *Nature,* **230,** 42–43.

Müller, R.D., Roest, W.R., Royer, J.-Y., Gahagan, L.M. & Sclater, J.G., 1997. Digital isochrons of the world's ocean floor, *J. geophys. Res.,* **102,** 3211–3214.

Mutter, J.C., Talwani, M. & Stoffa, P.L., 1982. Origin of seaward-dipping reflectors in oceanic crust off the Norwegian margin by 'subaerial seafloor spreading', *Geology,* **10,** 353–357.

Operto, S. & Charvis, P., 1996. Deep structure of the southern Kerguelen Plateau (southern Indian Ocean) from ocean bottom seismometer wide-angle data, *J. geophys. Res.,* **101,** 25 077–25 103.

Parson, T., McCarthy, J., Kohler, W.M., Ammon, C.J., Genz, H.M., Hole, J.A. & Criley, E.E., 1996. Crustal structure of the Colorado Plateau: application of a new long-offset seismic analysis technique, *J. geophys. Res.,* **101,** 11 173–11 194.

Pavlenkova, N.I., 1996. General features of the uppermost mantle stratification from long-range seismic profiles, *Tectonophysics,* **264,** 261–278.

Peirce, J.W., 1978. The northwards motion of India since the Late Cretaceous, *Geophys. J. R. astr. Soc.,* **52,** 277–312.

Peirce, J.W., Weissel, J.K. *et al.,* 1989. *Proc. ODP Init. Rept,* **121,** Ocean Drilling Program, College Station, TX.

Peterson, D.W. & Moore, R.B., 1987. Geological history and evolution of geological concepts, island of Hawaii, in *Volcanism in Hawaii,* eds Decker, R.W., Wright, T.L. & Stauffer, P.H., *USGS Prof Paper,* **1350,** 149–189.

Planke, S. & Eldholm, O., 1994. Seismic response and construction of seaward dipping wedges of flood basalts: Voring volcanic margin, *J. geophys. Res.,* **99,** 9263–9278.

Rees, B.A., Detrick, R.S. & Coakley, B., 1994. Seismic stratigraphy of the Hawaiian flexural moat, *Geol. Soc. Am. Bull.,* **105,** 189–205.

Royer, J.-Y., Peirce, J.W. & Weissel, J.K., 1991. Tectonic constraints on the hotspot formation of Ninetyeast Ridge, *Proc. ODP Init. Repts,* **121,** 763–776.

Saunders, A.D., Storey, M., Gibson, I.L., Leat, P., Hergt, J. & Thompson, R.N., 1991. Chemical and isotopic constraints on the origin of basalts from Ninetyeast Ridge: results from DSDP legs 22 and 26 and ODP leg 121, *Proc. ODP Init. Repts,* **121,** 559–584.

Schubert, G. & Sandwell, D., 1989. Crustal Volumes of the continents and of oceanic and continental submarine plateaus, *Earth planet. Sci. Lett.,* **92,** 234–246.

Smallwood, J.R., Staples, R.K., Richardson, K.R. & White, R.S., 1999. Crustal generation above the Iceland mantle plume: from continental rift to oceanic spreading center, *J. geophys. Res.,* **104,** 22 885–22 902.

Smith, W.H.F. & Sandwell, D.T., 1997. Global seafloor topography from satellite altimetry and ship soundings, *Science,* **277,** 1956–1962.

Staudigel, H. & Schmincke, H.-U., 1984. The Pliocene seamount series of La Palma, Canary Islands, *J. geophys. Res.,* **89,** 11 195–11 215.

Vidale, J.E., 1988. Finite-difference calculation of travel times, *Bull. seism. Soc. Am.,* **78,** 2062–2076.

Vidale, J.E., 1990. Finite-difference calculation of travel times in three dimensions, *Geophysics,* **55,** 521–526.

Watts, A.B. & Masson. D.G., 1995. A giant landslide on the north flank of Tenerife, Canary Islands, *J. geophys. Res.,* **100,** 24 487–24 498.

Watts, A.B., Peirce, C., Collier, J., Dalwood, R., Canales, J.P. & Henstock, T.J., 1997. A seismic study of lithosphere flexure in the vicinity of Tenerife, Canary Islands, *Earth planet. Sci. Lett.,* **146,** 431–447.

Watts, A.B., ten Brink, U.S., Buhl, P. & Brocher, T.M., 1985. A multichannel seismic study of the lithospheric flexure across the Hawaiian-Emperor seamount chain, *Nature,* **315,** 105–111.

Weigel, W. & Grevemeyer, I., 1999. The Great Meteor seamount: seismic structure of a submerged intraplate volcano, in *Hotspot and Oceanic Crust Interaction,* eds Charvis, P. & Danobeitia, J.J., *J. Geodyn.,* **28,** 27–40.

White, R.S. & McKenzie, D.P., 1989. The generation of volcanic continental margins and flood basalts, *J. geophys. Res.,* **94,** 7685–7729.

White, R.S., Spence, G.D., Fowler, S.R., McKenzie, D.P., Westbrook, G.K. & Bowen, A.N., 1987. Magmatism at rifted continental margins, *Nature,* **330,** 439–444.

White, R.S., McKenzie, D.P. & O'Nions, R.K., 1992. Oceanic crustal thickness from seismic measurements and rare earth element inversions, *J. geophys. Res.,* **97,** 19 683–19 715.

Wilson, J.T., 1963. Continental drift, *Sci. Am.,* **208,** 86–100.

Wolfe, C.J., McNutt, M.K. & Detrick, R.S., 1994. The Marquesas archipelagic apron: seismic stratigraphy and implications for volcano growth, mass wasting, and crustal underplating, *J. geophys. Res.,* **99,** 13 591–13 608.

Ye, S., Canales, J.P., Rihm, R., Danobeitia, J.J. & Gallart, J., 1999. A crustal transect through the northern and northeastern part of the volcanic edifice of Gran Canaria, Canary Islands, in *Hotspot and Oceanic Crust Interaction,* eds Charvis, P. & Danobeitia, J.J., *J. Geodyn.,* **28,** 3–26.

Zelt, C.A. & Ellis, R.M., 1988. Practical and efficient ray tracing in two-dimensional media for rapid travel time and amplitude forward modelling, *Can. J. expl. Geophys.,* **24,** 16–31.

Zelt, C.A. & Smith, R.B., 1992. Seismic travel times inversion for 2-D crustal velocity structure, *Geophys. J. Int.,* **108,** 16–34.